



HAL
open science

Negative-zero-positive metamaterial with omega-type inclusions

F. Zhang, G. Houzet, Eric Lheurette, D. Lippens, M. Chaubet, X. Zhao

► **To cite this version:**

F. Zhang, G. Houzet, Eric Lheurette, D. Lippens, M. Chaubet, et al.. Negative-zero-positive metamaterial with omega-type inclusions. *Journal of Applied Physics*, 2008, 103, pp.084312-1-8. 10.1063/1.2910831 . hal-00356921

HAL Id: hal-00356921

<https://hal.science/hal-00356921>

Submitted on 25 May 2022

HAL is a multi-disciplinary open access archive for the deposit and dissemination of scientific research documents, whether they are published or not. The documents may come from teaching and research institutions in France or abroad, or from public or private research centers.

L'archive ouverte pluridisciplinaire **HAL**, est destinée au dépôt et à la diffusion de documents scientifiques de niveau recherche, publiés ou non, émanant des établissements d'enseignement et de recherche français ou étrangers, des laboratoires publics ou privés.

Negative-zero-positive metamaterial with omega-type metal inclusions

Cite as: J. Appl. Phys. **103**, 084312 (2008); <https://doi.org/10.1063/1.2910831>

Submitted: 04 December 2007 • Accepted: 02 March 2008 • Published Online: 28 April 2008

Fuli Zhang, Gregory Houzet, Eric Lheurette, et al.



View Online



Export Citation

ARTICLES YOU MAY BE INTERESTED IN

[Electric-field-coupled resonators for negative permittivity metamaterials](#)

Applied Physics Letters **88**, 041109 (2006); <https://doi.org/10.1063/1.2166681>

[Ultra-broadband microwave metamaterial absorber](#)

Applied Physics Letters **100**, 103506 (2012); <https://doi.org/10.1063/1.3692178>

[Electric coupling to the magnetic resonance of split ring resonators](#)

Applied Physics Letters **84**, 2943 (2004); <https://doi.org/10.1063/1.1695439>

Lock-in Amplifiers
up to 600 MHz



Zurich
Instruments



Negative-zero-positive metamaterial with omega-type metal inclusions

Fuli Zhang,^{1,3} Gregory Houzet,¹ Eric Lheurette,¹ Didier Lippens,^{1,a)}
Michel Chaubet,² and Xiaopeng Zhao³¹*Institut d'Electronique de Micro-électronique et de Nanotechnologie, UMR CNRS 8520, University of Lille1, 59652, Villeneuve d'Ascq Cedex, France*²*Centre National d'Etudes Spatiales, 18 Avenue Edouard Belin, 31000, Toulouse, France*³*Department of Applied Physics, Northwestern Polytechnical University, Xi'an, 710072, People's Republic of China*

(Received 4 December 2007; accepted 2 March 2008; published online 28 April 2008)

We report on a negative-zero-positive metamaterial based on an omega-type microstructure with special attention on the nonvanishing group velocity for a zero refractive index. We first investigate the dispersion characteristics by full wave analysis, by stressing the necessary conditions of equality between the electric and magnetic plasma frequencies which are characteristic of the dispersion of the effective permittivity and permeability. Also, tuning of the gapless transition frequency between the left and right-handed dispersion branches was analyzed when the permittivity of the host substrate is changed. Last, we demonstrate experimentally the balanced composite character of the dispersion by frequency and angle-resolved transmission measurements, carried out at centimeter wavelengths on slabs and wedge-type prototypes, respectively.

© 2008 American Institute of Physics. [DOI: [10.1063/1.2910831](https://doi.org/10.1063/1.2910831)]

I. INTRODUCTION

The left-handed materials (LHMs), introduced by Veselago in 1968,¹ are now extensively studied to take benefit of unusual electromagnetic properties not found in natural materials. Basically, backward wave media can be synthesized either by introducing split ring resonator (SRR)/wire structures²⁻⁵ or other related particles such as omega-type arrays⁶⁻¹⁰ or by periodically loaded phase advance transmission lines,¹¹⁻¹⁵ as proposed in the pioneering book of Brillouin.¹⁶ For most LHMs, the left-handed (LH) passband is separated from the right-handed (RH) one by a band gap. At the edges of this passband, the group velocity vanishes. It was recently shown that a zero-gap dispersion characteristic can be achieved in LH transmission lines¹²⁻¹⁴ so that an infinite wavelength condition can be met at the wave vector $k=0$ with a nonvanishing group velocity. Such a structure was termed composite right and left-handed (CRLH) material, with an equality criterion between the series and parallel resonant frequencies of the lumped circuit elements. CRLH waveguides were used successfully at microwaves for sub-wavelength resonators and leaky wave antennas notably. The extension of the concept of balanced composite transmission lines to high-dimensionality devices such as metasurfaces and bulk metamaterials is a difficult task despite the encouraging results published recently.^{17,18}

In this paper, we investigate how the SRR/wire technology, which exhibits basically a narrow LH band separated by a forbidden gap from the RH one, can be used to realize a negative-zero-positive index material. To this aim, we based our analysis on an omega-type metal inclusion, which can be considered as a related compound of broadside coupled SRR/wire arrays so that the electric and magnetic responses can be treated as a whole. First, we show that under the

condition of interconnecting the omega-shaped particles, a broader band can be achieved, as demonstrated before by Kong's group.⁷⁻⁹ In a second stage, we identify the key geometrical parameters to balance the dielectric and magnetic plasma frequencies, and demonstrate the balanced composite character of the structure by the retrieval of the effective permittivity and permeability. These conclusions are then assessed experimentally by carrying out frequency and angle-resolved transmission measurements on slab and wedge-type prototypes operating at centimeter wavelengths.

The paper is organized as follows: In Sec. II, we analyze the guidelines to obtain a balanced composite metamaterial on the basis of plasma frequency analytical functions. The fitting of omega geometries is then performed by full-wave simulations, which permits us to deduce the complex k dispersion characteristics and to retrieve the refractive index, the Bloch impedance, along with the effective permittivity and permeability. In this section, we also consider the tunability of the dispersion characteristics. The properties of the microstructured slab and prismlike devices were numerically assessed using full-wave simulations and experimentally characterized by frequency and angle-resolved transmission measurements; the comparison is provided in Sec. III.

II. BALANCED STRUCTURE

A. Mode analysis

Figure 1 illustrates the typical dispersion of the effective permittivity and permeability of an edge-coupled split ring resonator/infinite wire and transmission response of one array whose basic cell is shown in the inset. In fact, an infinite wire array yields a quasi-Drude-type dependence for the dispersion of the effective permeability, whereas the effective permittivity of SRRs exhibits a Lorentz-type dispersion characteristic. It can be concluded that the material behaves as a

^{a)}Electronic mail: didier.lippens@iemn.univ-lille1.fr.

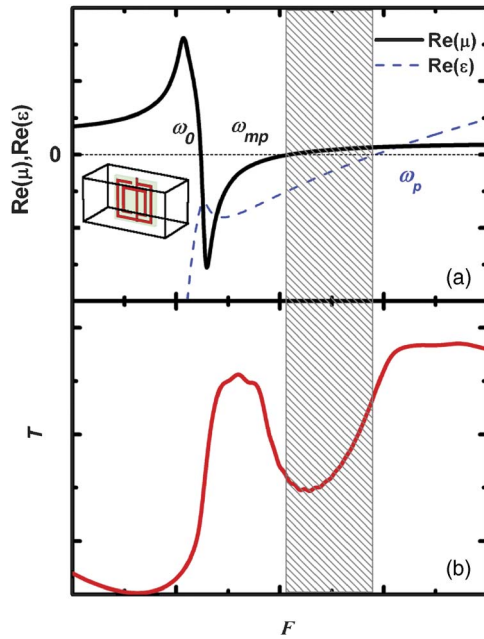


FIG. 1. (Color online) Characteristics of an edge-coupled SRR/wire (basic cell is shown in inset). (a) Real parts of permeability (solid) and permittivity (dash). (b) Frequency dependence of the transmission of an array. The band gap (gray region) ranging from ω_p and ω_{mp} is caused by a single negative effective parameter, i.e., negative permittivity.

single negative medium in the grayed frequency band between the magnetic plasma frequency ω_{mp} and the electric plasma frequency ω_p , within which the waves are evanescent. In contrast, the propagation is backward between the resonance frequency ω_0 (the magnetic resonance frequency of SRRs) and ω_{mp} and forward above ω_p .

Let us now consider an omega-type metal inclusion as depicted in Fig. 2. The basic unit cell [Fig. 2(a)] is composed of two Ω -patterns in a back-to-back configuration to avoid chiral effects.⁶ For pure magnetic excitation, namely for a magnetic dipole induced by the incident magnetic field (\mathbf{H}), the polarization of \mathbf{H} has to be along a direction normal to the surface on which the current loops (the C shape of the omega inclusion) are implemented. In addition, in order to induce an electrical activity, the E field polarization has to be oriented parallel to the arms of the omega patterns. Under these polarization considerations, the array was implemented according to the scheme shown in Fig. 2(b). A volumetric prototype is achieved by stacking several substrates with omega-shaped metal inclusions printed on one side of each layer. In order to alleviate a resonant characteristic in the dielectric response (quasi Drude-type dispersion), the omega arms are interconnected along the direction of the E field. As seen above, the plasma frequency ω_p is usually higher than the magnetic plasma frequency ω_{mp} for an unbalanced metamaterial. As a consequence, the condition of a balanced composite structure, achieved when $\omega_p = \omega_{mp}$, requires an increase of ω_{mp} or a decrease of ω_p .

In order to satisfy this criterion for omega-type arrays, we first considered a lumped-element circuit description of the magnetic response of the current loops^{9,10,19} and focused on some guidelines to achieve a balanced structure with negative-zero-positive behavior.

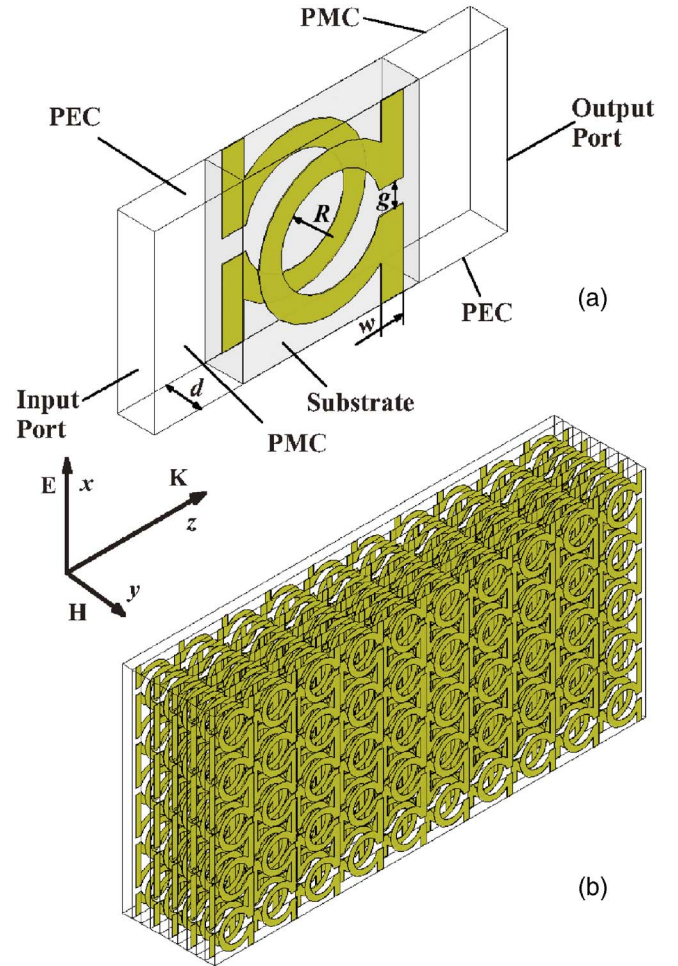


FIG. 2. (Color online) (a) Schematic of the omega unit cell. (b) Schematic of omega pattern array with an edge illumination by a plane wave.

For the current loops, the magnetic angular resonance frequency ω_0 can be described by the equation

$$\omega_0 = \frac{1}{\sqrt{LC}}, \quad (1)$$

where L is the inductance of the current loops and C is the total capacitance between the broadside coupled split ring resonators. Using a parallel-plate model, the total capacitance C (the fringing effect is not considered) is approximated by

$$C = \frac{1}{2}C_g = \frac{1}{2} \frac{\epsilon_0 \epsilon_r w}{d} \left(\pi \frac{2R+w}{2} - \frac{g}{2} \right), \quad (2)$$

where C_g is the capacitance between two half-circular rings of current loops, ϵ_0 and ϵ_r are the effective permittivity of the vacuum and substrate, respectively. w is the wire width, R is the inner radius, g is the gap of the omega pattern, and d is the thickness of the substrate. The inductance L of the omega pattern is given by

$$L = \mu_0 \pi R^2 / d. \quad (3)$$

The relation between the magnetic plasma frequency ω_{mp} and the resonant frequency ω_0 can be expressed as^{3,4}

$$\omega_{mp} = \frac{\omega_0}{\sqrt{1-F}}, \quad (4)$$

where $F = \pi R^2/S$ is the fraction occupied by the interior ring of the omega pattern in the xz plane and S is the area of the basic unit cell in the xz plane. On the other hand, the electric plasma frequency ω_p can be described in a first approximation by Pendry's formula as follows:²⁰

$$\omega_p^2 = \frac{2\pi c_0^2}{a^2 \ln(ar)}, \quad (5)$$

where a and r are the periodicity of the wire array and wire radius, respectively. It can be seen that the plasma frequency ω_p increases with the wire radius r . The cross section of wire considered here is rectangular whereas it was originally circular in Pendry's model, but the plasma frequency has an analogous function, i.e., increasing with the wire width w .²¹ Therefore, we see that reducing the strip width will cause an increase of ω_{mp} and a decrease of ω_p simultaneously, which could be employed as a rather simple method to achieve a balanced condition.

The aforementioned arguments can be used not only as a first estimate of the relevant geometry of the omega inclusions but also as guidelines to tune ω_{mp} and ω_p . However, because the magnetic and electric responses are not strictly separated, a finer optimization has to be conducted by means of a full-wave analysis. In practice, this procedure was performed with the HIGH FREQUENCY STRUCTURE SIMULATOR (HFSS) by Ansoft, a finite-element commercial software package. With respect to the numerical simulations reported below, it was found that the approximation of ω_{mp} by means of Eq. (4) is quite good (within a few percent), whereas Eq. (5) gives a more crude assumption of the plasma frequency due mainly to the difference in the wire array geometry. The dimensions of the basic unit cell were chosen as follows: $R = 1.1$, $w = g = 0.5$ (unit: millimeters). For these simulations, we assumed a substrate with the following dielectric characteristics at centimeter wavelength ($\epsilon_r = 4.0$, $\tan \delta = 0.02$) and a thickness of 0.8 mm. The basic cell dimensions are 3.9 mm along the x and z directions and 0.8 mm along y .

B. Balanced condition

The first clue for a zero-gap CRLH metamaterial is a broad transmission window which is assessed by the magnitude of the scattering parameter S_{21} . It is however difficult to conclude on the left-handedness or right-handedness of the dispersion characteristics. As a consequence, we calculated in the second stage the dispersion characteristics (Fig. 3) according to the method we used in Ref. 22 based on the Bloch-Floquet theorem. Note that this approach is similar to the retrieval method reported in Refs. 23 and 24. For this calculation, only one cell was considered along the propagation direction, whereas an infinitely long periodic array was mimicked along the transverse directions with proper boundary conditions [see Fig. 2(a)]. Perfect E conditions were applied for the surfaces normal to the omega arms, and perfect H boundaries to the surface parallels to the omega plane. In short, the solved scattering matrix is converted into the cor-

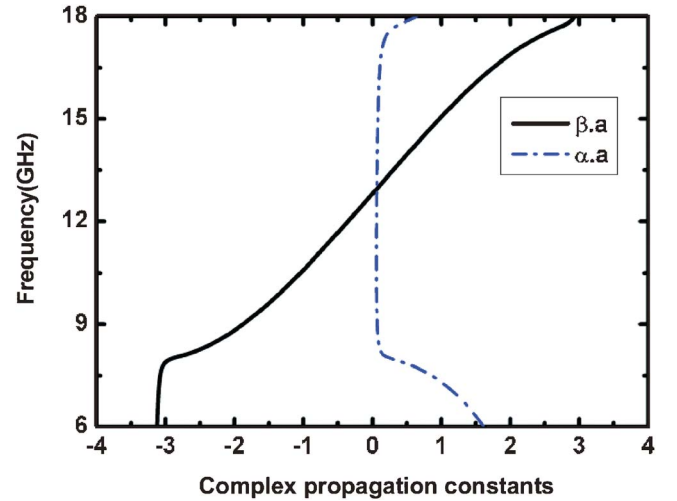


FIG. 3. (Color online) Dispersion characteristics of the negative-zero-positive index structure depicted in Fig. 2(b).

responding transfer matrix M , which is also termed an $ABCD$ or chain matrix. On the other hand, the chain matrix of a homogeneous propagation medium can also be written as a function of a complex propagation constant $\gamma = \alpha + j\beta$, where α and β depict the evanescence of the wave and the phase constant. z is the reduced impedance of the propagation medium with respect to its surrounding environment,

$$M = \begin{bmatrix} A & B \\ C & D \end{bmatrix} = \begin{bmatrix} ch(\gamma a) & z \cdot sh(\gamma a) \\ \frac{1}{z} \cdot sh(\gamma a) & ch(\gamma a) \end{bmatrix}. \quad (6)$$

By equating the various matrix elements of the microstructured and homogeneous media term by term, it can be shown that

$$\alpha = \frac{1}{a} \ln|A \pm \sqrt{A^2 - 1}|, \quad (7)$$

$$\beta a = \angle(A \pm \sqrt{A^2 - 1}) + 2k\pi, \quad k \in \mathbb{Z}, \quad (8)$$

$$z = \pm \sqrt{\frac{B}{C}}. \quad (9)$$

The information about the index is implicitly present in the complex propagation constant since

$$n = \frac{c\gamma}{i\omega}. \quad (10)$$

The dispersion characteristics of the real and imaginary parts of the propagation constant are displayed as a function of $\alpha \cdot a$ and $\beta \cdot a$ (a is the periodicity along the propagation direction; Fig. 2). It can be noted that the phase constant β is negative in the frequency domain in the 8.0–12.8 GHz frequency domain with a positive group velocity v_g ($\partial\omega/\partial\beta$). Hence, the group velocity and phase velocities of the propagating wave are antiparallel and therefore it supports a backward wave (LH mode). On the other hand, it supports a forward wave (RH mode) above 12.8 GHz. The corner frequency between the two modes is at 12.8 GHz, where the

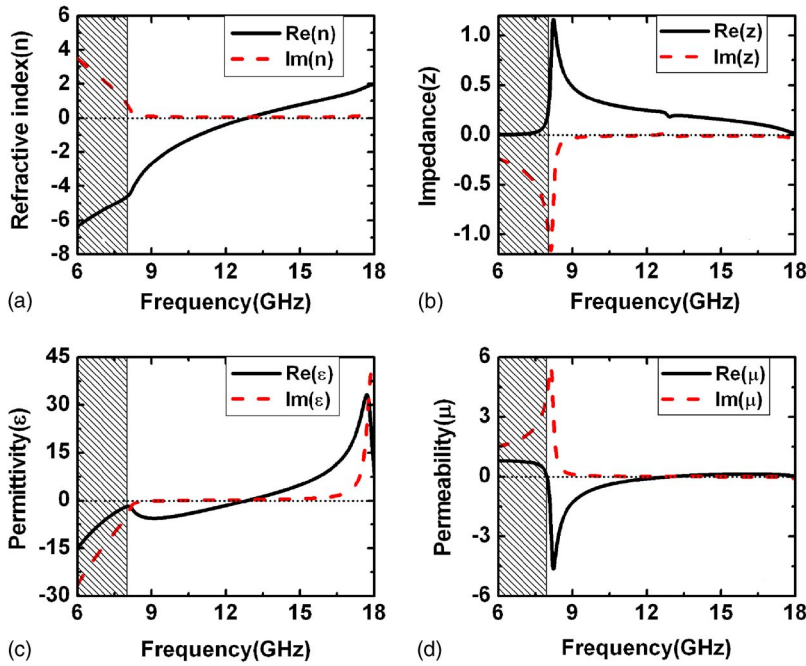


FIG. 4. (Color online) Effective parameters of negative-zero-positive structure retrieved from the scattering parameters of one unit cell. (a) Refractive index. (b) Impedance. (c) Permittivity. (d) Permeability.

phase constant is zero (infinite wavelength). In contrast with the conventional split ring resonator array (see Fig. 1), here the group velocity ($\partial\omega/\partial\beta$) does not vanish and presents a value close to 5.5×10^7 m s⁻¹ by taking an estimate of the slope at $k=0$. Below the resonant frequency of the current loops, corresponding to a forbidden gap, the evanescence of the waves is directly related to the decay length α^{-1} .

The variations of the Bloch impedance and of the refractive index, which can be determined from Eqs. (9) and (10), are plotted in Fig. 4. The physical meaning of n below ω_0 (gray region) is doubtful since the incident wave is evanescent. Just above ω_0 , a spike can be seen in the impedance resulting from the resonance effect. The refractive index exhibits a smooth transition between the negative band (8.0–12.8 GHz) and the positive band (12.8–16.0 GHz), with thus a transition frequency at 12.8 GHz where the refractive index value is zero. The frequency dependence of the effective permittivity can be described by a Drude model (continuous increase of the negative permittivity up to the electric plasma frequency). Although a slight resonant feature is superimposed at 8.1 GHz, the value of the effective permittivity is always negative. The effective permeability shows a well-defined negative peak at the resonance frequency with an increase in the losses. As a last comment, it can be assessed that the turning frequencies ω_{mp} and ω_p are equal.

C. Tunability of balanced structure

Because balanced structures enable smooth switching from the LH branch to the RH one, this opens the possibility to fabricate tunable balanced composite metamaterials. However, when some tunability is introduced, the magnetic plasma frequency ω_{mp} should always be equal to the plasma frequency ω_p in order to maintain the balanced condition, which considerably increases the difficulties. Basically, tunability can be introduced by changing the value of the ca-

pacitance C given by Eq. (2) via the modification of the unit cell geometry for fixed tuning or by varying the permittivity of the substrate. Such a tuning of ω_0 yields a concomitant shift of the magnetic plasma frequency ω_{mp} which varies as the inverse of the square root of the permittivity of the substrate according to Eq. (4).

For the frequency dependence of this artificial permittivity, we learned that the plasma frequency ω_p can also be described as the cutoff frequency of a metal wire array given by^{25,26}

$$\omega_p = C_{\text{light}}/2a\sqrt{\epsilon_r}, \quad (11)$$

where a is the periodicity of the wire array. From Eqs. (4) and (11), we see that both ω_{mp} and ω_p are proportional to $1/\sqrt{\epsilon_r}$. Therefore, the balanced condition will be independent of the permittivity of the substrate. In order to check this analysis, the influence of the substrate permittivity on the balanced condition was studied numerically. The results of this study in terms of dispersion characteristics are shown in Fig. 5. It is important to note that the balanced criterion is maintained when the permittivity of the substrate varies. The transition frequency increases gradually from 12.5 to 14.0 GHz as the permittivity is decreased from 4.2 to 3.4 with a step of 0.2. In summary, by incorporating some materials which exhibit a tunable permittivity, such as liquid crystals and ferroelectrics, it is possible to realize a reconfigurable balanced composite omega-based metamaterial.

III. EXPERIMENTAL RESULTS

In order to confirm experimentally the main conclusions of the previous theoretical analysis, we carried out two complementary studies. We first performed transmission measurements of a metamaterial slab in order to check the absence of a band gap between the LH and RH transmission window. The second type of transmission experiment was

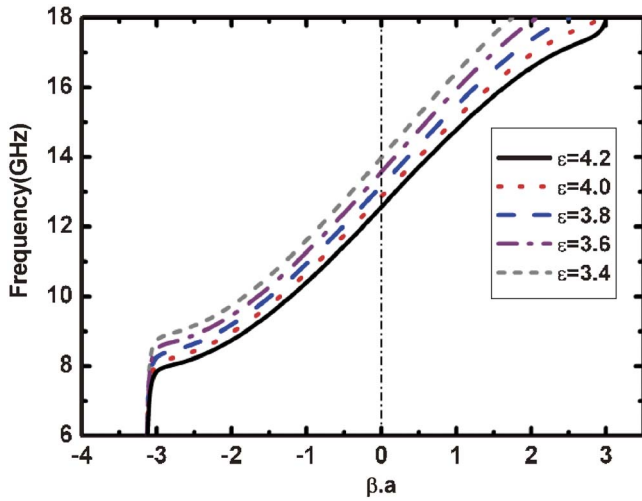
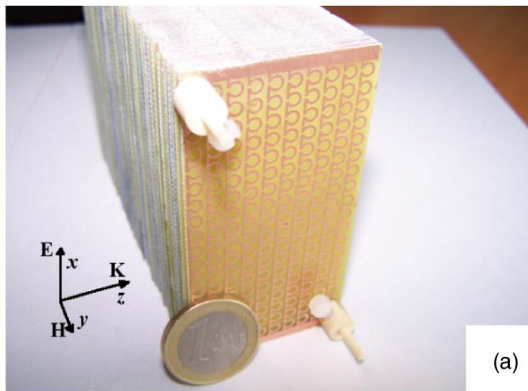


FIG. 5. (Color online) Propagation phase constant as a function of the substrate permittivity.

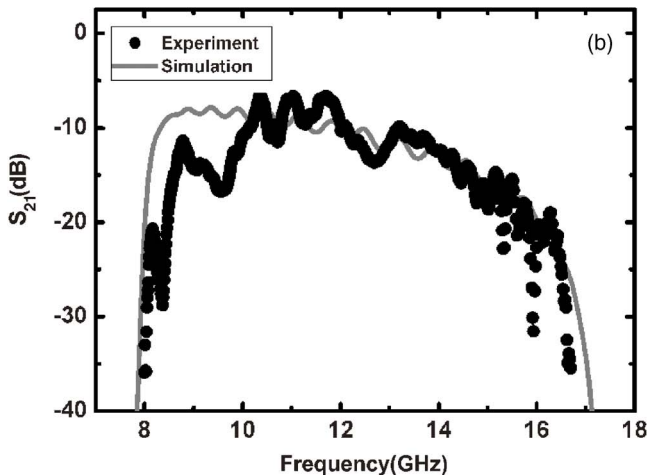
carried out on a prislake prototype under angle-resolved conditions, in order to determine the refractive index, via the Snell-Descarte's law.

A. Transmission measurement of the slab device

In practice, the metamaterial slab [Fig. 6(a)] consists of 100 layers of epoxy glass with omega patterns printed on one



(a)



(b)

FIG. 6. (Color online) Transmission measurement of the slab. (a) Photograph of slab sample fabricated for transmission measurements. (b) Transmission characteristics of the metamaterial slab.

side by the standard print circuit board (PCB) technology. Each layer consists of 10 unit cells along the z -direction and 18 unit cells along x with the same periodicity of 3.9 mm. Two horizontal strips were printed at the top and bottom edges of each layer to further increase the electrical length of the omega arms in order to avoid the influence of the wire finite length.²⁷

For the transmission experiment, the metamaterial slab was put between two aluminum plates with microwave absorbers on the side walls. This parallel plate waveguiding setup is similar to the one described in Ref. 28. The spacing between the aluminum plates fits the horn apertures equal to 7.5 cm. Two pairs of horns were used to initiate a Gaussian-shaped electromagnetic excitation at the input and to probe the transmitted signal at the output for the X band and K_u bands, respectively. We recall that the incident wave was set to propagate along the z -direction with the electric field along the x -direction and the magnetic field along y . The transmission spectrum was measured by an HP 85107A vector network analyzer.

Figure 6(b) compares the experimental and simulation transmission results. It can be seen that the slab exhibits a broad passband from 8.3–16.0 GHz, with a good agreement with the simulated transmission window. Despite the ripple resulting from the truncation of the structure, no band gap can be evidenced in the passband, which is consistent with the analysis of the dispersion curve of Fig. 2.

B. Angle-resolved measurement of the prislake device

For the refraction experiment, we have to ensure that a prislake structure can be used for the experimental determination of the refractive index n along the propagation direction. In fact, despite the fact that we fabricated a volumetric prototype, the structure properties are anisotropic so that the effective parameters are now described by tensors. This also explains why the previous slab cannot be used in a double-refraction experiment as carried out for isotropic metamaterial.

The model of the prism sample is depicted in Fig. 7. The incident beam impinges onto the sample at normal incidence with a Gaussian intensity profile tailored by side absorbers. For this condition of excitation, the electromagnetic wave undergoes refraction at the second tilted interface. Let us note that the prism model, which exhibits a stairlike pattern with a four-unit cell (eight omega patterns) step along the y -direction and a one-unit-cell along z , can be considered as a wedge of 30.5° . Seven stairs along the y -direction were found to be a good tradeoff between computer resources, accuracy, and reasonable calculation time. The prism was positioned between two perfect electric conductors (PEC), which sandwiched a unit cell in the x direction so that the structure can be considered infinite along this direction.

Figures 8(a)–8(c) shows the maps of the electric field magnitude at various operating frequencies calculated at the midplane between the top and bottom perfect electric conductors. The black arrow and the dash-dot line indicate the direction of the refracted beam and the normal to the second tilted interface, respectively. For a frequency of 10.0 GHz

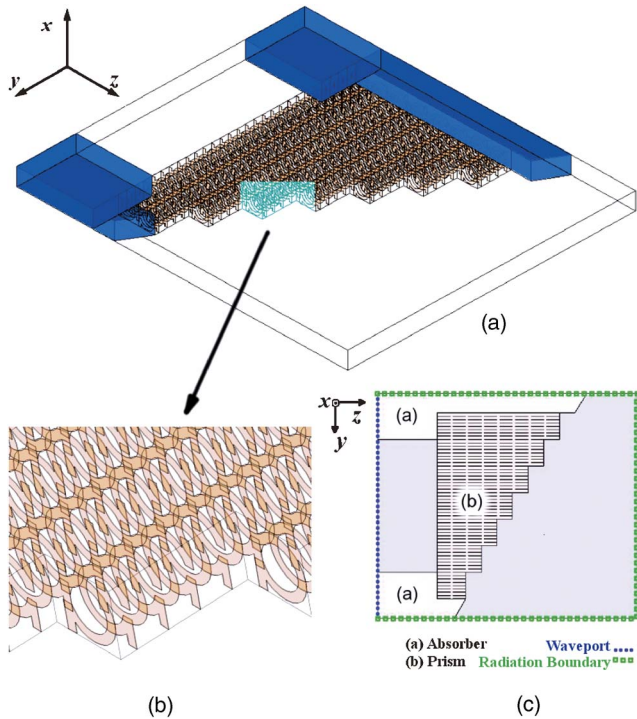


FIG. 7. (Color online) Prism model used in simulation. (a) 3D view of prism sample model. (b) Magnified view of one prism model stair, which consists of four cells along the y direction and one cell along the x direction. (c) Top view of prism model and applied boundaries.

[Fig. 8(a)], it can be seen that the angle of the refracted beam is in the negative direction with respect to the normal as expected for a LH dispersion branch. At 12.8 GHz [Fig. 8(b)], the refracted beam direction is quasiparallel to the normal, indicating that the refraction index is extremely close to zero. The magnitudes of the refracted beams at 12.8 and 10.0 GHz are comparable, thus in magnitude in agreement with the frequency dependence of the transmission of a slab shown in Fig. 5. Finally, at 15 GHz [Fig. 8(c)] the peak of the refracted beam is directed along a positive angle with respect to the normal and is consistent with the RH branch.

The prism refraction experiment was then carried out in a manner similar to the method reported in Ref. 2. The prism prototype, composed of 11 stairs instead of 7 for the simulation sample, is shown in Fig. 9(a). The number of unit cells along the propagation direction at the first stair and the last stair was increased to 5 and 15 cells, respectively. Figure 9(b) shows the normalized intensity of the refracted beam as a function of angular position of the probing horn antenna for three characteristic frequencies corresponding to a negative, zero, and positive index. By taking the central angle at the full width at half-maximum, the refraction beam peak was found to occur at -38.0° , 0.5° , and 13.0° , at 11.1, 13.6, and 15.0 GHz, respectively. Moreover, half the beamwidth of the refracted beam is only 15.9° at 13.5 GHz, which is smaller than that of 18.2° at 15.0 GHz and 29.2° at 11.1 GHz, consistent with the unique characteristics of a zero-index metamaterial.²⁹

The frequency dependence of the refractive index, computed from the Snell-Descartes' law, is plotted in Fig. 10(a). We see that the increase in the refractive index with fre-

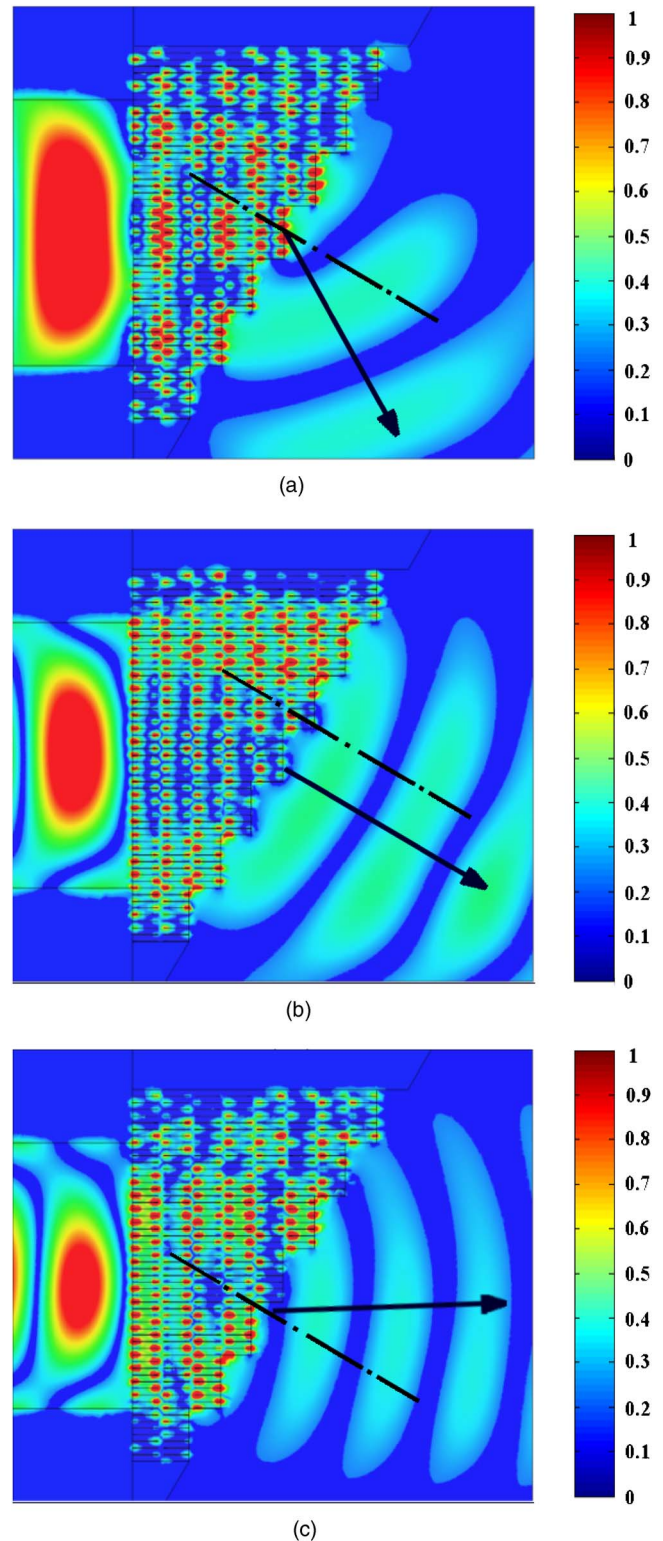


FIG. 8. (Color online) Electric field magnitude of refracted beam at different frequencies, (a) 10.0 GHz; (b) 12.8 GHz; (c) 15.0 GHz.

quency is continuous throughout the negative index to the positive index region. Thus, the experimental result demonstrates that the proposed structure indeed exhibits a balanced property with a negative-zero-positive behavior. The slight shift of the transition frequency between the experimental and numerical retrieved results is mainly due to the lower substrate permittivity in the simulation. However, it is noted

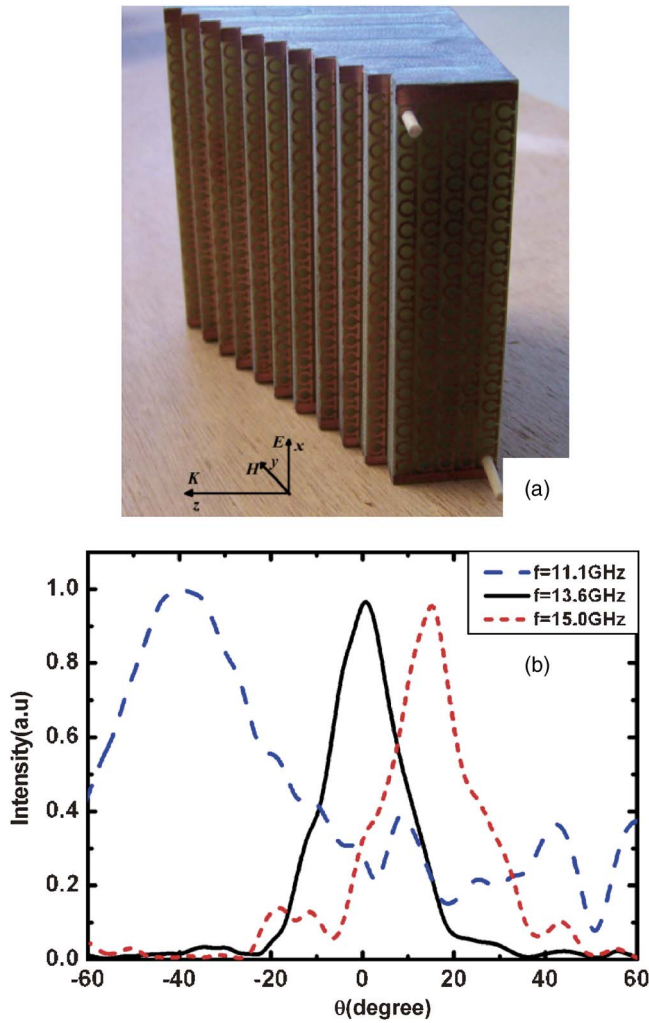


FIG. 9. (Color online) Experimental results of refraction measurement. (a) Photograph of the prismlike prototype. (b) Intensity of the refracted beam as a function of the probing horn angular position.

that the balanced condition is sustained because it does not depend on the substrate permittivity as shown in Fig. 5. Furthermore, the group velocity v_g of this metamaterial can also be obtained from the phase index $\text{Re}(n)$ as follows:^{16,30}

$$v_g = \frac{c}{\text{Re}(n) + \omega \frac{\partial \text{Re}(n)}{\partial \omega}}. \quad (12)$$

As shown in Fig. 10(b), the group velocity continuously decreases as the frequency is increased, indicating that the proposed structure is highly dispersive. For the transition frequency of 13.6 GHz, the group velocity is $4.8 \times 10^7 \text{ m s}^{-1}$, which clearly shows that energy can be transmitted through the device and offers the possibility to make use of the desired frequency point of zero refractive index.

IV. CONCLUSION

In summary, we have proposed a balanced composite LH/RH metamaterial based on omega-type structures. We experimentally and numerically demonstrated that this structure exhibits a broad transmission window from 8.3 to 16.0 GHz with a seamless transition frequency of 13.6 GHz from

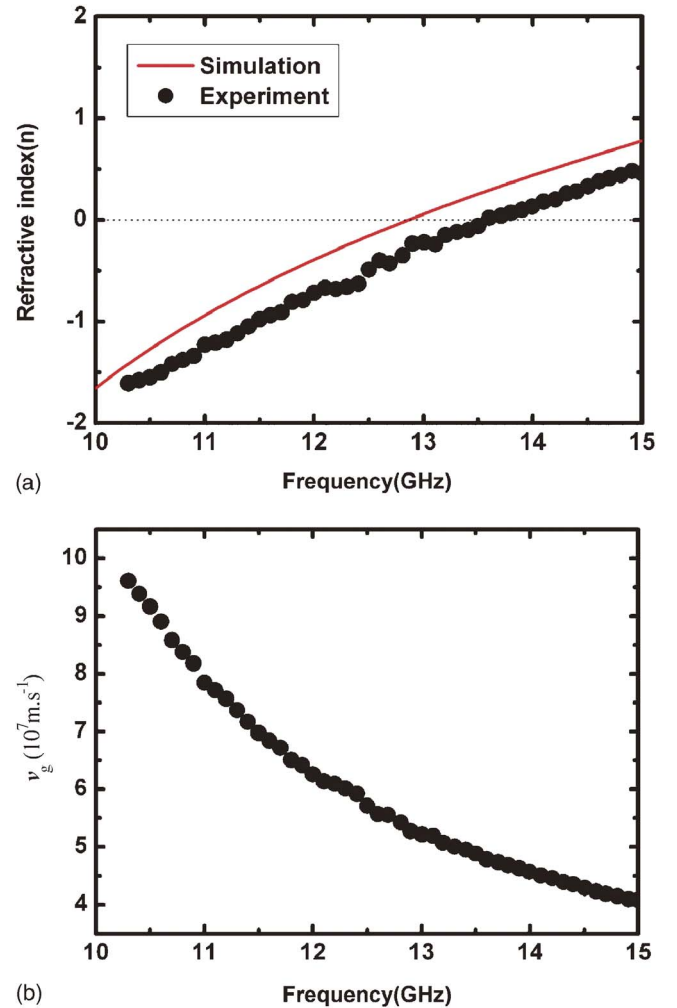


FIG. 10. (Color online) (a) Refractive index as a function of frequency. (b) Frequency dependence of the group velocity.

the LH to the RH dispersion branch. The balanced condition was demonstrated theoretically on the basis of the calculation of the dispersion characteristics and subsequent retrieval of the effective parameters. This was confirmed experimentally by means of frequency and angle-resolved transmission experiments carried out for a slab and prism prototype. The refractive index as well as the group velocity exhibits a continuous frequency dependence, notably at $k=0$ with a nonvanishing group velocity. The insensitivity of the balanced frequency to the tuning of the substrate permittivity makes the proposed architecture an interesting platform for steerable antennas at microwave frequencies.

ACKNOWLEDGMENTS

F. Zhang would like to acknowledge the China Scholarship Council for his fellowship. The authors would like to thank E. Delos and S. Potet for their help in microwave characterization.

¹V. G. Veselago, *Sov. Phys. Usp.* **10**, 509 (1968).

²R. Shelby, D. R. Smith, and S. Schultz, *Science* **292**, 77 (2001).

³D. R. Smith, W. J. Padilla, D. C. Vier, S. C. Nemat-Nasser, and S. Schultz, *Phys. Rev. Lett.* **84**, 4184 (2000).

⁴J. B. Pendry, A. J. Holden, D. J. Robbins, and W. J. Stewart, *IEEE Trans.*

- [Microwave Theory Tech.](#) **47**, 2075 (1999).
- ⁵F. Zhang, Q. Zhao, Y. Liu, C. Luo, and X. Zhao, [Chin. Phys. Lett.](#) **21**, 1330 (2004).
- ⁶C. R. Simovski and S. He, [Phys. Lett. A](#) **311**, 254 (2003).
- ⁷J. Huangfu, L. Ran, H. Chen, X. Zhang, K. Chen, T. M. Grzegorzczuk, and J. A. Kong, [Appl. Phys. Lett.](#) **84**, 1537 (2004).
- ⁸L. Ran, J. Huangfu, H. Chen, Y. Li, X. Zhang, K. Chen, and J. A. Kong, [Phys. Rev. B](#) **70**, 073102 (2004).
- ⁹L. Ran, J. Huangfu, H. Chen, X. Zhang, K. Cheng, T. M. Grzegorzczuk, and J. A. Kong, [Prog. Electromagn. Res.](#) **51**, 249 (2005).
- ¹⁰E. Lheurette, O. Vanbésien, and D. Lippens, [Microw. Opt. Technol. Lett.](#) **49**, 84 (2007).
- ¹¹A. Grbic and G. V. Eleftheriades, [Phys. Rev. Lett.](#) **92**, 117403 (2004).
- ¹²A. Lai, C. Caloz, and T. Itoh, [IEEE Microw. Mag.](#) **5**, 34 (2004).
- ¹³S. Lim, C. Caloz, and T. Itoh, [IEEE Trans. Microwave Theory Tech.](#) **53**, 161 (2004).
- ¹⁴A. Sanada, C. Caloz, and T. Itoh, [IEEE Microw. Wirel. Compon. Lett.](#) **14**, 68 (2004).
- ¹⁵T. Crepin, J. F. Lampin, T. Decoopman, X. Mélique, L. Desplanque, and D. Lippens, [Appl. Phys. Lett.](#) **87**, 104105 (2005).
- ¹⁶L. Brillouin, *Wave Propagation and Group Velocity* (Academic, New York, 1960).
- ¹⁷A. Grbic and G. V. Eleftheriades, [J. Appl. Phys.](#) **98**, 043106 (2005).
- ¹⁸P. Alitalo, S. Maslovski, and S. Tretyakov, [J. Appl. Phys.](#) **99**, 064912 (2006).
- ¹⁹R. Marques, F. Mesa, J. Martel, and F. Medina, [IEEE Trans. Antennas Propag.](#) **51**, 2572 (2003).
- ²⁰J. B. Pendry, A. J. Holden, W. J. Stewart, and I. Youngs, [Phys. Rev. Lett.](#) **76**, 4773 (1996).
- ²¹I. Bulu, H. Caglayan, and E. Ozbay, [Microw. Opt. Technol. Lett.](#) **48**, 2611 (2006).
- ²²T. Decoopman, O. Vanbesien, and D. Lippens, [IEEE Microw. Wirel. Compon. Lett.](#) **14**, 507 (2004).
- ²³D. R. Smith, D. C. Vier, T. Koschny, and C. M. Soukoulis, [Phys. Rev. E](#) **71**, 036617 (2005).
- ²⁴X. Chen, T. M. Grzegorzczuk, B.-I. Wu, J. Pacheco, and J. A. Kong, [Phys. Rev. E](#) **70**, 016608 (2004).
- ²⁵P. Markos and C. M. Soukoulis, [Phys. Rev. B](#) **65**, 033401 (2001).
- ²⁶X. Xu, Y. Xi, D. Han, X. Liu, J. Zi, and Z. Zhu, [Appl. Phys. Lett.](#) **86**, 091112 (2005).
- ²⁷T. Koschny, M. Kafesaki, E. N. Economou, and C. M. Soukoulis, [Phys. Rev. Lett.](#) **93**, 107402 (2004).
- ²⁸R. A. Shelby, D. R. Smith, S. C. Nemat-Nasser, and S. Schultz, [Appl. Phys. Lett.](#) **78**, 489 (2001).
- ²⁹S. Enoch, G. Tayeb, P. Sabouroux, N. Guérin, and P. Vincent, [Phys. Rev. Lett.](#) **89**, 213902 (2002).
- ³⁰J. F. Woodley and M. Mojahedi, [Phys. Rev. E](#) **70**, 046603 (2004).